4th International Conference on Computational and Mathematical Biomedical Engineering – CMBE2015
29 June - 1 July 2015, France
P. Nithiarasu and E.Budyn (Eds.)

THE IMPACT OF MINOR DOWNSTREAM ARTERIES ON UPSTREAM HAEMODYNAMICS: AN ILIAC ANEURYSM CASE STUDY

Lachlan J. Kelsey[1], Paul E. Norman[1,2], Janet T. Powell[3], Karol Miller[1] and Barry J. Doyle[1,4]
[1] Vascular Engineering, Intelligent Systems for Medicine Laboratory, The University of Western Australia, Australia. 20749083@student.uwa.edu.au; paul.norman@uwa.edu.au; karol.miller@uwa.edu.au; barry.doyle@uwa.edu.au
[2] School of Surgery, The University of Western Australia, Australia.
[3] Vascular Surgery Research Group, Imperial College London, UK. j.powell@imperial.ac.uk
[4] Centre for Cardiovascular Science, The University of Edinburgh, UK.

SUMMARY

The accuracy and usefulness of computed flow data in an artery is dependent on the initial geometry, which is in turn dependent on image quality. Often smaller branching vessels are not captured with CT, and thus neglected in flow simulations. We used a high-quality CT dataset of an isolated common iliac aneurysm, where the small branching vessels of the internal iliac artery were evident. Simulations were performed both with and without these branches. Results show that the haemodynamics in both cases were very similar and therefore, small downstream arteries may not be vital to accurate computations of upstream flow.

Key words: *iliac aneurysm, computational fluid dynamics, wall shear stress*

1 INTRODUCTION

An aneurysm is a localised dilation of an artery wall which is life threatening when ruptured. Aneurysms in the iliac arteries can occur in isolation, or in association with other large vessel aneurysms, such as abdominal aorta or femoral artery aneurysms. Large-scale population screening studies of abdominal aortic aneurysms (AAA) show that, for people older than 65 years, the prevalence of an AAA is approximately 5–6% in men and 1–2% in women. In 25% of these cases, sufferers also have aneurysms in one or both common iliac arteries; and in 7% of these cases aneurysms also exist in the internal iliac arteries. However, the underlying causes of most aneurysms in these medium-to-large arteries are unknown and specific pathological causes are generally only identified in a small number of cases [1].

In the past decades computational fluid dynamics (CFD) has emerged as a powerful and popular tool for the study of blood flow dynamics and its role in the development, diagnosis, and treatment of aneurysms and related cardiovascular disease [2,3]. With appropriate boundary conditions and model assumptions, CFD can simulate the blood flow through any vessel of the body using patient-specific geometries, typically derived from computed tomography (CT). However, CT imaging methods have limited spatial resolution (e.g. 1 mm voxel size) and in many studies the minor arteries are lost or excluded from the models, reducing their fidelity.

For this case study we have an exceptional geometry, reconstructed from a patient with a common iliac aneurysm (CIA). The geometry contains a number of the minor arteries, branching from the internal iliac arteries; these minor arteries are often not-captured by CT and neglected in CFD studies of the normal or diseased aortic bifurcation. The objective of this case study is to analyse the effect that these minor arteries (present versus not present) (Figure 1) have on the haemodynamics and physical flow phenomena commonly associated with aneurysmal disease: specifically regions of low and oscillatory wall shear stress (WSS).

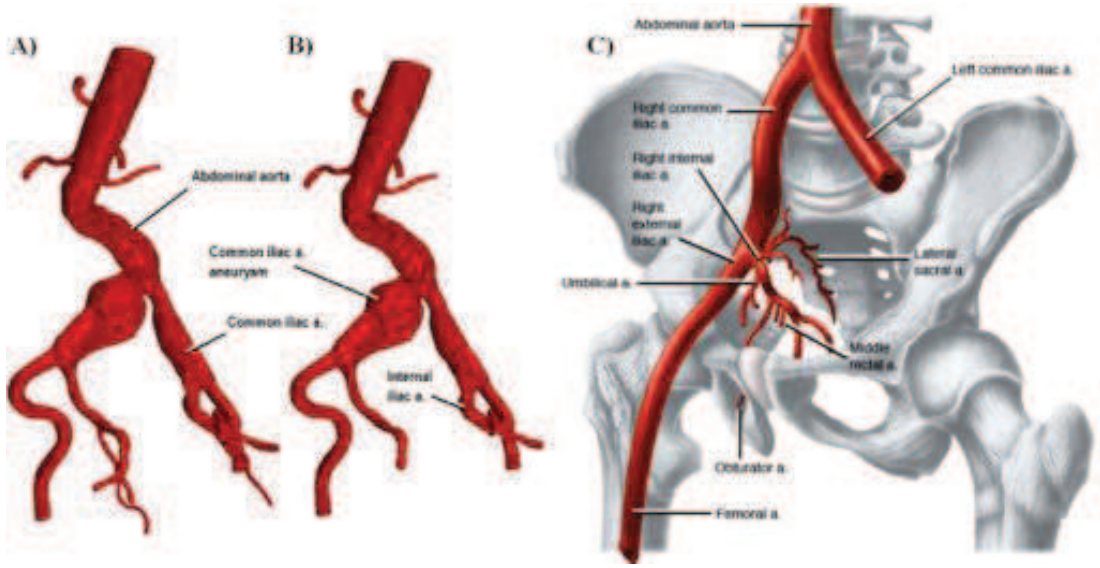

Figure 1: A) Original CT-reconstructed geometry. B) Trimmed geometry. C) Healthy anatomy of the iliac arteries. (a. = artery)

2 METHODOLOGY

2.1 3D reconstruction and trimming

Contrast-enhanced CT data (pixel size = 0.82mm; slice thickness = 1 mm) of a 91 year old male with an isolated CIA was imported into Mimics v17 (Materialise, Belgium). Following previous methods, we reconstructed the lumen into 3D and conservatively smoothed the resulting surfaces [3]. The patient had a 'pocket' within the CIA lumen which was expected to produce complex flow. The trimmed geometry was created by removing all branching arteries from the internal iliac arteries. We created an outlet boundary where the rectal and obturator arteries once were on the patient's non-aneurysmal side, as the internal iliac artery progressed directly into these minor arteries. We then extended the inlet surface by 120 mm and each outlet by 10 times the outlet diameter to ensure flow was fully developed entering the infra-renal aorta and that our outlet boundary conditions did not affect the haemodynamics in the vessels. The resulting reconstructions can be seen in Figure 1.

2.2 Meshing

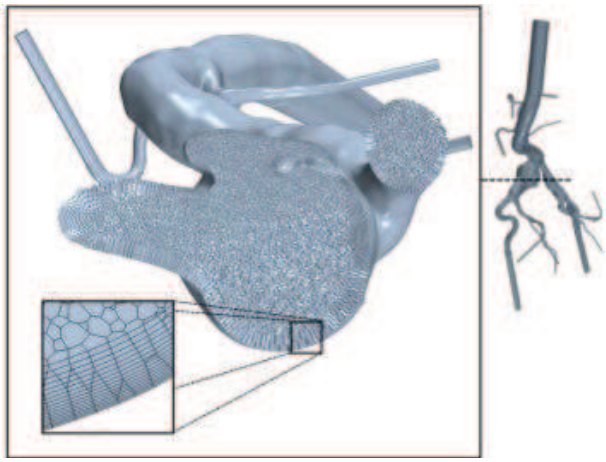

Figure 2: Mesh cross-section through the CIA 'pocket', highlighting the prism-layer mesh and local mesh refinement.

The volume mesh was constructed within STAR-CCM+ (v9.04) (CD-adapco Group) using a core polyhedral mesh and a prism-layer mesh near the wall boundary. The prism-layer mesh was progressively refined approaching the wall. The thickness of the prism-layer mesh and the surface size (edge length) were defined relative to the local lumen diameter so that the minor arteries were well discretised. Any areas that were expected to have rapid changes in velocity (i.e. bifurcations) were also subject to refinement. In order to determine a sufficient level of (uniform) mesh refinement (number of prism-layers and polyhedra density coefficient) the Grid Convergence Index (GCI) was calculated from the results of three different mesh densities (using the untrimmed geometry). The GCI calculated for the time-averaged WSS, spatially-averaged over the cells spanning the CIA was 0.08% (<2% is considered robust). The finest and chosen mesh (Figure 2) contained 16 prism-layers and a total cell count of 5.8 million (4.8 million for the trimmed geometry).

2.3 Physical assumptions and boundary conditions

The blood flow was approximated as laminar and the blood was considered to be an incompressible, Newtonian fluid with a dynamic viscosity of 0.0035 Pa·s and a density of 1050 kg/m^3. The walls of the arteries were characterised by no-slip, rigid wall boundary conditions [2, 3]. For both the original and trimmed geometries, the Navier-Stokes equations were solved using STAR-CCM+. The temporal discretization was set to second order, with 10^3 steps per cardiac cycle and 15 inner iterations: the convergence of both the continuity and momentum residuals remained below 10^{-3} throughout the cardiac cycle. A mass flow waveform was applied at the supraceliac (SC) inlet, this scaled waveform was derived from volumetric flow data by Les et al. [4] (Figure 3).

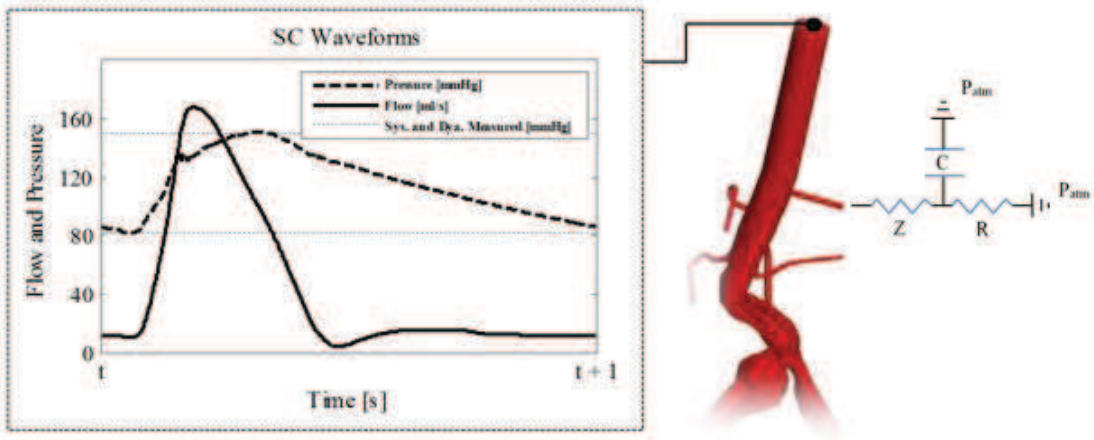

Figure 3: Left: SC inlet waveforms and the patient's systolic and diastolic blood pressures. Right: An example of the Windkessel Model used at each outlet boundary, where Z is the proximal resistance, R is the distal resistance and C is the vascular compliance. P_{atm} is atmospheric pressure.

The model explicitly couples the 3D CFD simulation with a Windkessel model (RCR circuit) at each outlet boundary (Figure 3) in order to approximate the resistance and compliance of the downstream vascular beds. This improves the estimation of pressure throughout the domain and allows the pressure waveform at the SC inlet to be set-to/abide-by the patient's measured systolic and diastolic pressures [4]. The Windkessel parameters are calibrated according to previous methodology [5], with 30% of the common iliac flow passing through to the internal iliac artery. Furthermore, downstream of each internal iliac artery, the flow leaving the domain is split (directly) proportional to the area of each outlet boundary and the shape of the flow waveform leaving each of the iliac outlets is configured to resemble the infrarenal aortic waveform. These assumptions are often used as patient-specific flow and pressure data for each outlet are not routinely collected.

2.4 Data Analysis

Once the pressure waveform at the inlet converged to the desired systolic and diastolic pressures, the time-averaged WSS (TAWSS) and oscillatory shear index (OSI) were calculated over three cardiac cycles. Following this, histograms were used to quantify the distribution of TAWSS and OSI across the areas of interest: the common and internal iliac arteries. The characteristics of the flow in these regions were observed by time-averaging the velocity profile across plane sections.

3 RESULTS

Throughout both the geometries, there were only slight differences in the TAWSS and OSI distributions. The results show extremely low TAWSS (at <0.4 Pa we expect monocyte adhesion and inflammation [6]) and a high OSI at the aneurysmal location, in particular, within the 'pocket' (Figure 4). In Figure 5 we see the area-weighted distribution of TAWSS over the CIA region. This histogram reinforces the similarity seen in Figure 4 and is characteristic of the marginal differences in TAWSS and OSI that were observed throughout both geometries. There was, however, slightly more variation observed in the average velocity profiles, most prominent for the section through the CIA 'pocket' where the flow field is the most complex. Although this bares less significance than the TAWSS and OSI fields, it is effective in highlighting how far upstream the changes made

have affected the flow field. Also, we observed very little difference in flow dynamics in the internal iliac artery where the trimmed geometry resembled the original geometry with respect to flow features, TAWSS and OSI.

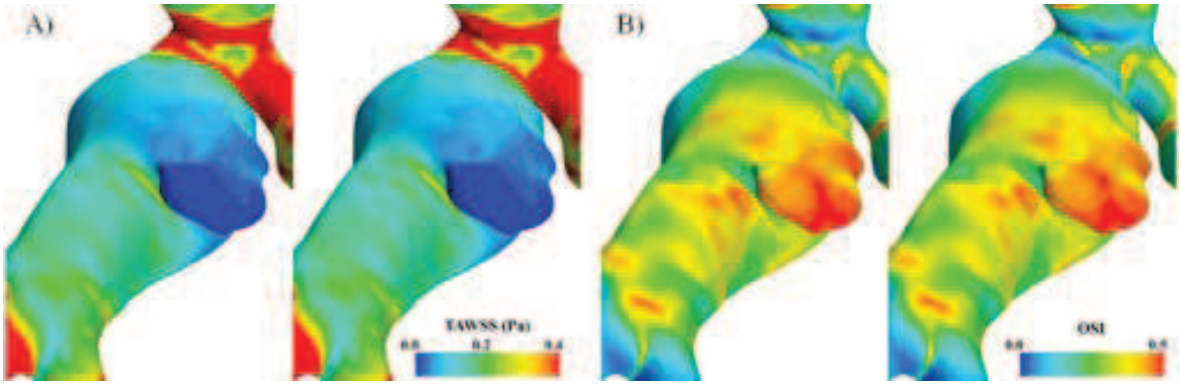

Figure 4: A) TAWSS distribution (left: original geometry, right: trimmed geometry). B) OSI distribution (left: original geometry, right: trimmed geometry).

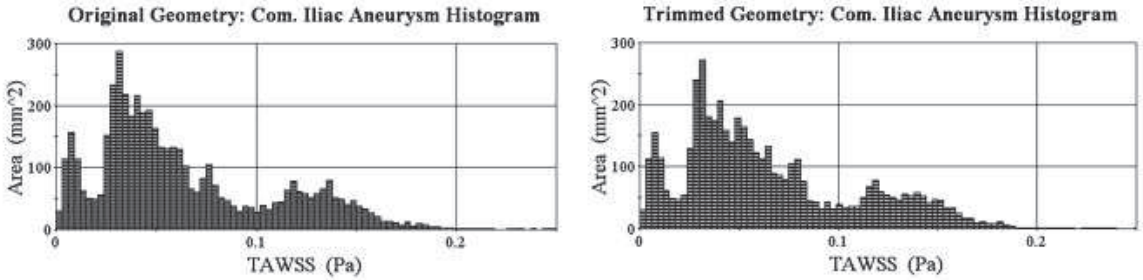

Figure 5: Area-weighted TAWSS histograms for the CIA region in both the original (left) and trimmed geometry (right).

4 CONCLUSION

Logically, the accuracy with which a CT reconstruction captures the true in vivo anatomy will have implications on the computed flow field. However, the inclusion of the smaller branch beyond the carotid bifurcation (i.e. the superior thyroid artery) was shown to insignificantly affect the flow in the common carotid artery [7]. Here, in the diseased aortic bifurcation, we came to a similar conclusion. By employing a typical set of large artery CFD assumptions that omit smaller branching vessels, we observed negligible qualitative or quantitative differences in computed flow dynamics in the CIA or the internal iliac artery. This work validates the omission of smaller branches of the internal iliac artery and forms the basis for a larger investigation into isolated CIAs.

REFERENCES

[1] P.E. Norman and J.T. Powell. Site Specificity of Aneurysmal Disease. Circ, 121:560-8, 2010.
[2] D.A. Steinman, et al. Variability of Computational Fluid Dynamics Solutions for Pressure and Flow in a Giant Aneurysm: The ASME 2012 Summer Bioengineering Conference CFD Challenge. J Biomech Eng, 135(2): 021016-1-13, 2013.
[3] B.J. Doyle, et al. From Detection to Rupture: A Serial CFD Study of a Rapidly-Expanding, Patient-Specific, Ruptured AAA. In: B.J. Doyle, K. Miller, A. Wittek, P.M.F. Nielson (Eds), Computational Biomechanics for Medicine: Fundamental Science and Patient-Specific Applications, 5-68, 2014.
[4] A.S. Les, et al. Supraceliac and Infrarenal Aortic Flow in Patients with AAAs: Mean Flows, Waveforms, and Allometric Scaling Relationships. Cardiovasc Eng Technol, 1(1): 39–51, 2010.
[5] A.S. Les, et al. Quantification of Hemodynamics in AAAs During Rest and Exercise Using MRI and CFD. Ann Biomed Eng, 38(4): 1288-1313, 2010.
[6] D. Hardman et al. On the Prediction of Monocyte Deposition in Abdominal Aortic Aneurysm Using Computational Fluid Dynamics. J Eng Med, 227(10): 1114-1124, 2013.
[7] S.Z. Zhao et al. Flow in Carotid Bifurcations: Effect of the Superior Thyroid Artery. Med Eng Phys, 21(4): 207-214, 1999.